Journal of Nuclear Medicine, published on June 8, 2017 as doi:10.2967/jnumed.117.189779

Molecular imaging of human embryonic stem cells stably expressing human PET reporter genes after zinc finger nucleases-mediated genome editing.

Authors: Esther Wolfs[1]‡*, Bryan Holvoet[1*], Laura Ordovas[2,3], Natacha Breuls[1,4], Nicky Helsen[2,3], Matthias Schönberger[5], Susanna Raitano[2,3], Tom Struys[6], Bert Vanbilloen[1], Cindy Casteels[1], Maurilio Sampaolesi[4], Koen Van Laere[1], Ivo Lambrichts[6], Catherine M. Verfaillie[2,3]*, Christophe M. Deroose[1]*

Affiliations:
[1]Nuclear Medicine & Molecular Imaging and Molecular Small Animal Imaging Centre, Department of Imaging and Pathology, KU Leuven, Leuven, Belgium.
[2]Stem Cell Institute, KU Leuven, Leuven, Belgium.
[3]Department of Development and Regeneration, Stem Cell Biology and Embryology, KU Leuven, Leuven, Belgium.
[4]Translational Cardiomyology Lab, Department of Development and Regeneration, KU Leuven, Leuven, Belgium.
[5]Department of Pharmaceutical and Pharmacological Sciences, KU Leuven, Leuven, Belgium.
[6]Biomedical Research Institute, Morphology Research Group, Lab of Histology, Universiteit Hasselt, Diepenbeek, Belgium.

*Authors contributed equally to this manuscript.

‡Current affiliation: Biomedical Research Institute, Morphology Research Group, Lab of Histology, Universiteit Hasselt, Diepenbeek, Belgium

Corresponding author: Prof. dr. Christophe Deroose
UZ Leuven, Division of Nuclear Medicine
Campus Gasthuisberg, Herestraat 49, B-3000 Leuven
+3216343712
christophe.deroose@uzleuven.be

First author: Dr. Esther Wolfs
Biomedical Research Institute, UHasselt
Agoralaan, Gebouw C, B-3590 Diepenbeek
+3211269277
Esther.wolfs@uhasselt.be

Short title: ESC imaging after genome editing

ABSTRACT

Rationale. Molecular imaging is indispensable for determining the fate and persistence of engrafted stem cells. Standard strategies for transgene induction involve the use of viral vectors prone to silencing and insertional mutagenesis or the use of non-human genes.

Methods. We used zinc finger nucleases (ZFN) to induce stable expression of human imaging reporter genes into the safe harbor locus adeno-associated virus integration site 1 (*AAVS1*) in human embryonic stem cells (ESC). Plasmids were generated carrying reporter genes for fluorescence, bioluminescence imaging (BLI), and human positron emission tomography (PET) reporter genes.

Results. *In vitro* assays confirmed their functionality and ESC retained differentiation capacity. Teratoma formation assays were performed and tumors were imaged over time with PET and BLI.

Conclusions. This study demonstrates the application of genome editing for targeted integration of human imaging reporter genes in human ESC for long-term molecular imaging.

Key Words: Genome Editing, Stem Cells, Reporter Genes, PET, Noninvasive Imaging

INTRODUCTION

For further development of stem cell-based therapies, long-term non-invasive imaging of grafted cells is indispensable for determining their fate and viability. Therefore, non-invasive imaging reporter genes are a suitable tool for long-term tracking of grafted stem cells (*1*).

Previous research has attempted to deliver exogenous genes into the genome of ESC and induced pluripotent stem cells using various strategies (*2*). However, long-term follow-up of grafted cells is difficult due to signal silencing (*3,4*). Furthermore, random and multiple integrations in the host cell genome can perturb the biological properties and stability of cells resulting in a non-isogenic cell population (*5*).

Genome editing approaches have recently been developed for an efficient targeting approach without random or multiple integrations within the genome of the host cells (*6*). One example is the use of ZFN (*7-10*) which contain specific recognition sites up to 36bp coupled to a FokI endonuclease domain generating DNA double strand breaks upon dimerization. This is repaired by either non-homologous end joining or homologous recombination if a donor plasmid carrying the genes of interest is provided flanked by homologous sequences to the regions next to the double strand break. This results in the introduction of the sequence of interest into the host cell genome (*5,7*).

ZFN have been designed and used to target the *AAVS1* locus, encoding the ubiquitously expressed protein phosphatase 1 regulatory subunit 12C (PPP1R12C) gene located on chromosome 19 (*11,12*). The *AAVS1* locus is a “safe harbor” locus as the integration of target genes in this locus does not evoke pathological responses (*13*) nor perturbs the proliferation,

karyotype or expression of pluripotency genes in ESC and induced pluripotent stem cells (*7,14*). In addition, when ESC are differentiated the inserted gene is not silenced.

Here, the *AAVS1* locus of ESC was used to introduce a construct carrying reporter genes for non-invasive imaging. Enhanced green fluorescent protein (*eGFP*) was introduced for histological validation. Firefly luciferase (*Fluc*) was included for BLI (*15*). Finally, a radionuclide imaging reporter gene was included in the construct; either the human sodium iodide symporter (h*NIS*) or the human somatostatin receptor subtype 2 (h*SSTr2*). As the insertion site lies downstream of exon 1 of a transcribed gene, a promoterless puromycin resistance cassette was included into the donor construct to maximize the selection efficiency of correctly targeted cells (*14*).

The paradigm reporter gene for PET is the herpes simplex virus type 1 thymidine kinase (*HSV1-TK*) (*16-19*). This reporter gene has allowed non-invasive documentation in animal models of *in vivo* gene transfer, cell monitoring and protein-protein interactions (*20*), and has also been used in clinical applications (*17-19*). Its gene product might be immunogenic; furthermore, if treatment with antiviral drugs is necessary, the *HSV1-TK*-mediated conversion of the prodrug to its cytotoxic form causes unwanted cell death. Finally, substrates for *HSV1-TK* might require nucleoside transporters to incorporate the PET probe in the cells and alterations in transporter status could influence the PET signal.

h*NIS* is commonly used for single photon emission computed tomography (SPECT), PET and radionuclide therapy of the thyroid gland due to its ability to transport radioactive forms of iodine and other negatively charged ions into thyroid cells (*21,22*). h*NIS* is principally present in

the thyroid. Other tissues such as the stomach mucosa, mammary glands or the salivary glands also express h*NIS* at lower levels (*22*). This implies a low background signal for radionuclide imaging and partly contributes to the interest in the application of h*NIS* as a PET reporter gene (*23*).

The h*SSTr2* has been imaged for years in the clinic for detection of neuroendocrine tumors using ^{111}In-pentetreotide or gallium-68 labeled peptides such as ^{68}Ga-DOTA-octreotate (^{68}Ga-DOTATATE) (*24*). These molecules are commercially available or are in widespread use for neuroendocrine tumor imaging (*25*). This receptor is predominantly expressed in the gastrointestinal tract including the pancreas, the spleen as well as in the pituitary gland (*24,26*).

The goal of this study was to generate a stably expressing ESC line for non-invasive, longitudinal multimodality imaging with human PET reporter genes through genome editing with a ZFN-mediated approach.

MATERIALS AND METHODS

Cell culture

The human ESC line H9 (WA09) was purchased from WiCell Research Institute. ESC were maintained feeder-free using mTeSR1 medium (StemCell Technologies, Vancouver, Canada).

Generation of reporter cell lines

The pZ:puro-CAGGS-*eGFP*-P2A-*Fluc*-T2A-h*NIS*-plasmid and the pZ:puro-CAGGS-*eGFP*-P2A-*Fluc*-T2A-h*SSTr2*-plasmid were generated using the pZ-donor *AAVS1* vector (CompoZr Targeted Integration Kit, Sigma Aldrich, MO, USA).

ESC were resuspended in nucleofection solution 2 (Amaxa, Lonza, Basel, Switzerland) with 10µg donor plasmid and 3µg ZFN mRNA per $2x10^6$ cells. Cells were electroporated using program F16. After a week of puromycin selection, individual clones were expanded resulting in two reporter cell lines: $hNIS^+$ and $hSSTr2^+$ ESC.

Polymerase chain reaction (PCR) genotyping

Genomic DNA was extracted using the QIAamp DNA mini kit (Qiagen, Venlo, The Netherlands) following the manufacturers protocol.

To check for reporter gene incorporation, junction assays were performed at the 5' and 3' end of the target locus. Random integrations were checked using primers at 5' and 3' sites next to the cassette. The wild-type allele was amplified with primers at the sites adjacent to the insertion site to determine whether the integration was mono- or bi-allelic. Primer sequences can be found in Table 1.

Southern blot

Genomic DNA was digested with EcoRI and loaded onto a 0.7% agarosegel. Fragments were transferred to a nylon membrane (Zeta-probe; Biorad, California, US) which was UV-cosslinked and prehybridization was performed. Digoxigenin (DIG; Roche, Basel, Switzerland) labeling of the probe targeting the homology arm was done by PCR using the donor vector. Hybridization of the membrane with the probe was performed using the DIG High Prime DNA Labelling and Detection starter Kit II (Roche) according to manufacturer's instructions.

Hepatic differentiation

Hepatic differentiation of ESC was performed as previously described (*27*).

In vitro validation of reporter gene expression

In vitro BLI was performed as previously described (*28*).

ESC were plated, washed and incubated with tracer solution (0.74MBq/mL) for 1h. $^{99m}TcO_4^-$ and iodide ($^{124}I^-$, Perkin Elmer, Waltham, MA, USA) were used for h*NIS*$^+$ ESC and ^{68}Ga-DOTATATE for h*SSTr2*$^+$ ESC. Cells were washed 3 times and tracer concentration in the cell fraction was measured using a gamma counter (Wizard, Perkin Elmer). Values were corrected for cell numbers. h*NIS* Blocking was performed with $NaClO_4$ (0.74MBq/ml $^{99m}TcO_4^-$ in 10µM $NaClO_4$) and h*SSTr*2 blocking with cold octreotide (0.74MBq/ml ^{68}Ga-DOTATATE in 0.08, 0.25, 0.74, 2.2, 6.7, 20, 60nM octreotide). Efflux of $^{99m}TcO_4^-$ was measured by incubating cells with $^{99m}TcO_4^-$ for 1h, followed by incubation with tracer-free medium for 5, 15, 30, 60 and 120 minutes. Saturation experiments were performed by incubation of h*SSTr2*$^+$ ESC with different solutions of ^{68}Ga-DOTATATE (0.015MBq/mL; 0.022MBq/ml; 0.11MBq/ml; 0.37MBq/ml or 2.22MBq/ml). Each condition included a blocking with cold octreotide (20nM). Cells were incubated for 10 minutes and activities in the cells were measured after 3 washing steps. Based on activity inside the cell and specific activity the amount of ^{68}Ga-DOTATATE bound to the cells was calculated.

Real-time quantitative PCR

Gene expression analysis of pluripotency markers and ESC differentiation towards the hepatic lineage was performed using RT-qPCR as previously described(*27*). Primer sequences are listed in Table 2.

Immunostaining

Stainings were performed as described previously (*28*). Goat anti-eGFP (1:500, Abcam), goat anti-Oct4 (1:200, Abcam, Cambridge, UK), rabbit anti-Nanog (1:200, Abcam), goat anti-Sox2 (1:50, Santa Cruz Biotechnology, Dallas, USA) and mouse anti-TRA1-60 (1:50, Santa Cruz) were used. Anti-rabbit, anti-goat and anti-mouse Alexa Fluor®594 (1:500 in 1% BSA, Thermo Fisher) or anti-goat Alexa Fluor®488 (1:500, Thermo Fisher) secondary antibodies were used.

Animal preparations

All animal protocols were approved by the Ethical Committee of the KU Leuven. 8-week old female BALB/c Rag2$^{-/-}$ɣc$^{-/-}$ mice were anesthetized with 2% isoflurane (Isoflurane ISP®, Rothacher, Basel, Switzerland). 3-5x10^{6} ESC were resuspended 1:1 in PBS and Matrigel (BD biosciences). h*SSTr2*$^{+}$ ESC were injected on the left flank and h*NIS*$^{+}$ ESC contralaterally (n=8).

Bioluminescence imaging

BLI was performed as previously described(*28*).

^{68}Ga-DOTATATE preparation

See online supplemental files.

Small-animal PET

Imaging was performed on day 1, 22 and day 63, after intravenous injection of ~3.7MBq of ^{68}Ga-DOTATATE or ^{124}I^{-} per mouse (n≥5), with static acquisitions of 20min using a Focus

220 microPET system (Siemens Medical Solutions USA, Knoxville,TN). Time after injection was 1h for ^{68}Ga-DOTATATE and 2h for $^{124}I^-$.

Images were reconstructed with a maximum a posteriori image reconstruction algorithm and analyzed using PMOD 3.0 (PMOD technologies, Zürich, Switzerland). Images were converted to standardized uptake value (SUV).

A manually delineated volume of interest was positioned around the teratomas. Ratios were calculated comparing the signal to the contralateral tumor.

Histological processing

Masson's trichrome staining was performed using standard protocols and analyzed to identify the presence of derivatives of the three germ layers.

Statistical analysis

Data are presented as mean ± standard error of the mean. Analysis of variance analysis was performed. P-values <0.05 were considered statistically significant. Data were processed using GraphPad Prism version 5.00 for Windows (GraphPad Software, San Diego, California, USA).

RESULTS

Generation of reporter cell lines

Two reporter gene constructs were generated, flanked by 800bp stretches of homology to the ZFN target site *AAVS1*, downstream of exon 1 of the *PPP1R12C* gene on chromosome 19 (Fig. 1A). The reporter genes were *eGFP, Fluc* allowing BLI and either the h*NIS* or the h*SSTr2* reporter gene for PET and/or SPECT.

PCR genotyping, Southern blot and expression of pluripotency markers

PCR genotyping was performed to assess proper integration of the construct and to exclude random integrations (Fig. 1A). Both h*SSTr2*$^{+}$ and h*NIS*$^{+}$ colonies carried the expression cassette as confirmed by the 5' and 3' junction assays. Single or bi-allelic integration of the cassette was assessed. In both clones, bi-allelic integration into the *AAVS1* locus was observed. No random integrations had occurred.

Correct integration of the expression construct was confirmed with Southern blot. One single band was present depicting bi-allelic integration (Fig. 1A). The expression of pluripotency markers *OCT4, NANOG, SOX2* and *KLF4* was assessed and no difference in expression was observed compared to WT ESC (Fig. 1B). Immunocytochemistry for *OCT4, NANOG, SOX2 and TRA1-60* showed a similar expression in all lines (Fig. 1C).

Hepatic differentiation

WT, h*SSTr2*$^{+}$ and h*NIS*$^{+}$ ESC showed a similar differentiation capacity towards the hepatic lineage (Fig. 2). The expression of hepatocyte-specific genes *HNF4α, AFP, Albumin* and *A1AT* increased in both cell lines. No significant difference was observed between the WT and the genome-edited ESC. The definitive endoderm markers *EOMES, MIXL1, CXCR4* and *SOX17* were expressed similarly in all cell lines.

In vitro validation of reporter gene expression

Genome-edited cells, before and after differentiation, had significantly higher BLI signals compared to WT ESC (Fig. 3A; $p<0.05$).

Functionality of h*SSTr2* and h*NIS* was tested with radioligand uptake experiments. After one hour, 52.1% of $^{99m}TcO_4^-$ was taken up per $5x10^5$ h*NIS*$^+$ ESC, 50-80 times more than controls ($p=0.001$). $NaClO_4$ reduced uptake levels significantly (0.77%). h*NIS*$^+$ hepatocytes maintained an uptake of 40.7%, not significantly different from undifferentiated cells (52.1%; $p>0.05$) (Fig. 3B). A decreased tracer retention was observed, although after 1h ~20% of the tracer remained intracellularly (Fig. 3C).

h*SSTr2*$^+$ ESC could bind 3.18% per million cells of the ^{68}Ga-DOTATATE, 6.9 times more than h*NIS*$^+$ cells ($p<0.001$). h*SSTr2*$^+$ hepatocytes maintained their ^{68}Ga-DOTATATE binding capacity. Octreotide administration caused a fourfold reduction of the ^{68}Ga-DOTATATE uptake (0.77%; $p<0.001$) (Fig. 3D). An IC_{50} value of 0.58nM was demonstrated (Fig. 3E). A saturation experiment showed a Bmax value of 111±5fmol per million cells and Kd of 3.4±0.5nM (Fig. 3F).

In vivo noninvasive longitudinal imaging

BLI of h*SSTr2*$^+$ and h*NIS*$^+$ teratomas showed a robust signal that increased over 70 days (Fig. 4). Small-animal PET was performed on day 1, 22 and 63 (Fig. 5). A focus of increased ^{68}Ga-DOTATATE accumulation was observed at the h*SSTr2*$^+$ teratoma. No increased ^{68}Ga-DOTATATE uptake was seen at the site of the h*NIS*$^+$ teratoma. On day 1 the h*SSTr2*$^+$ ESC showed 3.07±0.84 times more signal than the h*NIS*$^+$ ESC ($p<0.01$). This signal increased significantly to 5.02±2.0 times more signal in the h*SSTr2*$^+$ ESC on day 63 (Fig. 5A).

On the first day after engraftment of the h*NIS*$^+$ ESC a focus of increased tracer uptake was observed with 2.87±1.0 times more accumulation of $^{124}I^-$ than the h*SSTr2*$^+$ teratomas

($p<0.001$). On day 63 after engraftment the signal increased significantly to 4.66±0.7 times more tracer uptake in h*NIS*$^+$ teratomas compared to the controls ($p<0.05$) (Fig. 5B).

Teratoma assay

Histological examination confirmed teratoma formation and thus maintenance of pluripotency after ZFN targeting. Teratomas from both lines contained cells derived from the three different germ layers (Online supplemental Fig. 1). h*SSTr2*$^+$ teratomas formed neural rosettes, cartilage and intestinal lining epithelium. h*NIS*$^+$ teratomas were less dense and contained more fluid overall containing neural rosettes, cartilage and glandular tissue. Immunohistochemistry confirmed expression of h*SSTr2* and h*NIS* in h*SSTr2*$^+$ and h*NIS*$^+$ teratomas, respectively.

DISCUSSION

The delivery of genetic material into cells has mainly been done through the use of viral vectors. Hence, insertional mutagenesis may occur resulting in the disruption of the host genetic material and there is a potential risk for oncogenesis. Furthermore, non-isogenic cell lines are generated. The primary transduced cell population is a heterogeneous mix of cells which are all genomically different from each other. Furthermore, reporter gene silencing is dependent on the integration site. These factors can result in signal loss and confound data interpretation (*29,30*).

In this work we used the innovative ZFN-mediated approach for genetic engineering of ESC. Human PET imaging reporter genes were introduced into the *AAVS1* locus which is known to be a so-called safe harbor locus (*7,13,14*). *AAVS1* has a continuously open chromatin structure

with insulator elements that prevents epigenetic silencing and thereby allows stable transgene expression, at least when a transgene is expressed from a constitutive active promoter (*7,14*).

This technology is very translational as two major limitations of stem cell imaging are tackled at once. ZFN provide safe and controlled introduction of genetic material. Second, human PET reporter genes will not evoke immune responses. The tracers required for these genes are available in routine clinical use and do not require an on-site cyclotron. We used two reporter constructs for multimodal imaging enabling the monitoring of cells after injection using BLI and PET or SPECT.

In this study we show the efficient introduction of the reporter cassette in both alleles of the *AAVS1* locus. Very high *in vitro* uptake ratios are reached (~2 orders of magnitude higher than WT controls) and *in vivo* imaging is possible when the xenograft is not yet detectable by clinical examination.

h*NIS* is a symporter protein and thus mediates an amplification of the imaging signal (*22,31*). After their uptake through h*NIS*, no organification of tracer molecules occurs which leads to a partial leakage (*28*). Nevertheless, h*NIS* has many advantages such as its human origin, its low background expression and the availability of a number of tracer molecules that are compatible. Receptors such as the h*SSTr2* as imaging reporter proteins bind one single ligand in a 1:1 ratio with high affinity (*32*). No signal amplification or tracer leakage will occur, but the h*SSTr2* is of human origin and is characterized by low endogenous expression outside some specific endocrine organs.

Both imaging reporter genes have their disadvantages, but due to their evident advantages, they are very good candidates to be used as imaging reporter genes. The choice of

the reporter gene will be mainly based on the anatomical location to be imaged, depending on their endogenous expression.

BLI and small-animal PET was performed on h*SSTr2*$^{+}$ and h*NIS*$^{+}$ ESC injected subcutaneously. BLI showed robust signal intensities which further increased specifically. PET signals increased significantly over time and more predominantly in h*SSTr2*$^{+}$ ESC teratomas. h*NIS*$^{+}$ teratomas contained more fluid-containing cysts not contributing to the signal. h*SSTr2*$^{+}$ teratomas were more dense causing a relatively higher PET signal.

With ^{68}Ga-DOTATATE PET, mean SUV values of 0.07±0.03 in h*SSTr2*$^{+}$ and 0.03±0.02 in h*NIS*$^{+}$ teratomas were observed (Fig. 5A). ^{124}I^{-} PET led to mean SUV values of 0.21±0.08 and 0.06±0.01 in h*NIS*$^{+}$ and *SSTr2*$^{+}$ teratomas, respectively (Fig. 5B). Imaging of metastasis in a mouse model using melanoma cells expressing *HSV1-TK* imaged with ^{18}F-FHBG resulted in a mean uptake of 3.3%ID/g (SUV~0.9, formula from (*33*)). Hepatoma and rat glioma cells expressing *HSV1-TK* reporter led to ~1.6%ID/g and ~0.7%ID/g 1-2 weeks after engraftment with ^{14}C-FIAU and ^{18}F-FHBG,(*34*), implying SUV values of ~0.32 and ~0.14. Prostate cancer cells expressing HSV1-TK resulted in an uptake of 0.2%ID/g, or a SUV of 0.04 (*35*). Our data suggest slightly lower SUV values, however, others have used transfection or transduction to insert the reporter genes. Hence, multiple copies are inserted leading to higher expression levels. In our work, one single copy of the reporter gene is included into the genome, and a lower expression level is inevitable. Also in h*SSTr2*$^{+}$ teratomas, lower SUV values were obtained because of similar reasons. Furthermore, lower receptor densities were observed in comparison with (*36*). To circumvent this, antagonists can be used as they are able to bind more h*SSTr2* sites (*36,37*).

Histological examination confirmed that ZFN targeting does not alter the pluripotency of the ESC. Furthermore, *in vitro* hepatic differentiation of h*SSTr2*$^{+}$ and *hNIS*$^{+}$ ESC was equally efficient compared to WT ESC.

Our results are in line with those of Wang et al. who introduced *Fluc*, monomeric red fluorescent protein and *HSV1-TK* in the *AAVS1* locus of ESC and induced pluripotent stem cells (*38*). A high efficiency of the targeting procedure was shown with preservation of pluripotency, differentiation capacity and long-term gene expression. The survival of the cells was monitored with BLI but not with PET. Also, the gene product of *HSV-TK* is foreign to the human species and might imply immunological consequences and unwanted cell death.

CONCLUSION

We demonstrate the introduction of human radionuclide reporter genes into the genome of human ESC in a safe and controlled manner using the innovative ZFN-mediated strategy, thereby surpassing possible immune reactions against the imaging reporter genes. Furthermore, we long-term imaged ZFN-engineered ESC using reporter gene small-animal PET. Isogenic cell lines were generated and these cells could be fully characterized for patient applications. Off-target effects were described (*39,40*), but the search for novel strategies has led to the discovery of the CRISPR/Cas (clustered regulatory interspaced short palindromic repeats) system (*41*). It is clear that genetic engineering in the field of stem cell imaging can greatly accelerate the transition of basic research to a clinical setting, and these innovative techniques can therefore be used in order to explore other human PET reporter genes.

DISCLOSURE

CMD and KVL are senior clinical investigators of the Flemish Fund for Scientific Research (FWO). CC is a post-doctoral fellow of the FWO. BH and NB are PhD students funded by IWT. LO was funded by IWT/OZM/090838, IACS BPAMER3/08/04, and Government of Aragon FMI048/08. Funding to CMV was from FWO G.0667.07 and G.0975.11; KU Leuven (ETH-C1900-PF, EME-C2161-GOA/11/012), IWT-HEPSTEM and IWT-HILIM-3D, BELSPO-IUAP-DEVREPAIR, FP7-HEMIBIO (266777).

ACKNOWLEDGEMENTS

We thank Manja Muijtjens, Pieter Berckmans, Jeanine Santermans and Ann Van Santvoort for their help in data acquisition and processing. Radiopharmacy from Nuclear Medicine UZ Leuven is acknowledged for ^{68}Ga-DOTATATE preparations.

REFERENCES

1. Yaghoubi SS, Campbell DO, Radu CG, Czernin J. Positron emission tomography reporter genes and reporter probes: gene and cell therapy applications. *Theranostics.* 2012;2:374-391.

2. Giudice A, Trounson A. Genetic modification of human embryonic stem cells for derivation of target cells. *Cell Stem Cell.* 2008;2:422-433.

3. Herbst F, Ball CR, Tuorto F, et al. Extensive methylation of promoter sequences silences lentiviral transgene expression during stem cell differentiation in vivo. *Mol Ther.* 2012;20:1014-1021.

4. Krishnan M, Park JM, Cao F, et al. Effects of epigenetic modulation on reporter gene expression: implications for stem cell imaging. *FASEB J.* 2006;20:106-108.

5. Collin J, Lako M. Concise review: putting a finger on stem cell biology: zinc finger nuclease-driven targeted genetic editing in human pluripotent stem cells. *Stem Cells.* 2011;29:1021-1033.

6. Li M, Suzuki K, Kim NY, Liu GH, Izpisua Belmonte JC. A cut above the rest: targeted genome editing technologies in human pluripotent stem cells. *J Biol Chem.* 2014;289:4594-4599.

7. Hockemeyer D, Soldner F, Beard C, et al. Efficient targeting of expressed and silent genes in human ESCs and iPSCs using zinc-finger nucleases. *Nat Biotechnol.* 2009;27:851-857.

8. Lombardo A, Genovese P, Beausejour CM, et al. Gene editing in human stem cells using zinc finger nucleases and integrase-defective lentiviral vector delivery. *Nat Biotechnol.* 2007;25:1298-1306.

9. Zou J, Maeder ML, Mali P, et al. Gene targeting of a disease-related gene in human induced pluripotent stem and embryonic stem cells. *Cell Stem Cell.* 2009;5:97-110.

10. Raitano S, Ordovas L, De Muynck L, et al. Restoration of progranulin expression rescues cortical neuron generation in an induced pluripotent stem cell model of frontotemporal dementia. *Stem Cell Reports.* 2015;4:16-24.

11. Kotin RM, Linden RM, Berns KI. Characterization of a preferred site on human chromosome 19q for integration of adeno-associated virus DNA by non-homologous recombination. *EMBO J.* 1992;11:5071-5078.

12. Tan I, Ng CH, Lim L, Leung T. Phosphorylation of a novel myosin binding subunit of protein phosphatase 1 reveals a conserved mechanism in the regulation of actin cytoskeleton. *J Biol Chem.* 2001;276:21209-21216.

13. Smith JR, Maguire S, Davis LA, et al. Robust, persistent transgene expression in human embryonic stem cells is achieved with AAVS1-targeted integration. *Stem Cells.* 2008;26:496-504.

14. DeKelver RC, Choi VM, Moehle EA, et al. Functional genomics, proteomics, and regulatory DNA analysis in isogenic settings using zinc finger nuclease-driven transgenesis into a safe harbor locus in the human genome. *Genome Res.* 2010;20:1133-1142.

15. Keyaerts M, Caveliers V, Lahoutte T. Bioluminescence imaging: looking beyond the light. *Trends Mol Med.* 2012;18:164-172.

16. Gambhir SS, Bauer E, Black ME, et al. A mutant herpes simplex virus type 1 thymidine kinase reporter gene shows improved sensitivity for imaging reporter gene expression with positron emission tomography. *Proc Natl Acad Sci U S A.* 2000;97:2785-2790.

17. Jacobs A, Voges J, Reszka R, et al. Positron-emission tomography of vector-mediated gene expression in gene therapy for gliomas. *Lancet.* 2001;358:727-729.

18. Penuelas I, Mazzolini G, Boan JF, et al. Positron emission tomography imaging of adenoviral-mediated transgene expression in liver cancer patients. *Gastroenterology.* 2005;128:1787-1795.

19. Yaghoubi SS, Jensen MC, Satyamurthy N, et al. Noninvasive detection of therapeutic cytolytic T cells with 18F-FHBG PET in a patient with glioma. *Nat Clin Pract Oncol.* 2009;6:53-58.

20. Paulmurugan R, Massoud TF, Huang J, Gambhir SS. Molecular imaging of drug-modulated protein-protein interactions in living subjects. *Cancer Res.* 2004;64:2113-2119.

21. Van Sande J, Massart C, Beauwens R, et al. Anion selectivity by the sodium iodide symporter. *Endocrinology.* 2003;144:247-252.

22. Dohan O, De la Vieja A, Paroder V, et al. The sodium/iodide Symporter (NIS): characterization, regulation, and medical significance. *Endocr Rev.* 2003;24:48-77.

23. Penheiter AR, Russell SJ, Carlson SK. The sodium iodide symporter (NIS) as an imaging reporter for gene, viral, and cell-based therapies. *Curr Gene Ther.* 2012;12:33-47.

24. Deroose CM, Hindie E, Kebebew E, et al. Molecular imaging of gastroenteropancreatic neuroendocrine tumors: current status and future directions. *J Nucl Med.* 2016;57:1949-1956.

25. Serganova I, Ponomarev V, Blasberg R. Human reporter genes: potential use in clinical studies. *Nucl Med Biol.* 2007;34:791-807.

26. Reubi JC, Kvols L, Krenning E, Lamberts SW. Distribution of somatostatin receptors in normal and tumor tissue. *Metabolism.* 1990;39:78-81.

27. Roelandt P, Vanhove J, Verfaillie C. Directed differentiation of pluripotent stem cells to functional hepatocytes. *Methods Mol Biol.* 2013;997:141-147.

28. Wolfs E, Holvoet B, Gijsbers R, et al. Optimization of multimodal imaging of mesenchymal stem cells using the human sodium iodide symporter for PET and Cerenkov luminescence imaging. *PLoS One.* 2014;9:e94833.

29. Ellis J. Silencing and variegation of gammaretrovirus and lentivirus vectors. *Hum Gene Ther.* 2005;16:1241-1246.

30. Ramachandra CJ, Shahbazi M, Kwang TW, et al. Efficient recombinase-mediated cassette exchange at the AAVS1 locus in human embryonic stem cells using baculoviral vectors. *Nucleic Acids Res.* 2011;39:e107.

31. Ahn BC. Sodium iodide symporter for nuclear molecular imaging and gene therapy: from bedside to bench and back. *Theranostics.* 2012;2:392-402.

32. Cotugno G, Aurilio M, Annunziata P, et al. Noninvasive repetitive imaging of somatostatin receptor 2 gene transfer with positron emission tomography. *Hum Gene Ther.* 2011;22:189-196.

33. Phelps ME. *PET: Molecular Imaging and Its Biological Applications*: Springer New York; 2012.

34. Min JJ, Iyer M, Gambhir SS. Comparison of [18F]FHBG and [14C]FIAU for imaging of HSV1-tk reporter gene expression: adenoviral infection vs stable transfection. *Eur J Nucl Med Mol Imaging.* 2003;30:1547-1560.

35. Yang H, Berger F, Tran C, Gambhir SS, Sawyers CL. MicroPET imaging of prostate cancer in LNCAP-SR39TK-GFP mouse xenografts. *Prostate.* 2003;55:39-47.

36. Reubi JC, Schar JC, Waser B, et al. Affinity profiles for human somatostatin receptor subtypes SST1-SST5 of somatostatin radiotracers selected for scintigraphic and radiotherapeutic use. *Eur J Nucl Med.* 2000;27:273-282.

37. Reubi JC, Waser B, Macke H, Rivier J. Highly increased 125I-JR11 antagonist binding in vitro reveals novel indications for sst2 targeting in human cancers. *J Nucl Med.* 2017;58:300-306.

38. Wang Y, Zhang WY, Hu S, et al. Genome editing of human embryonic stem cells and induced pluripotent stem cells with zinc finger nucleases for cellular imaging. *Circ Res.* 2012;111:1494-1503.

39. Cathomen T, Joung JK. Zinc-finger nucleases: the next generation emerges. *Mol Ther.* 2008;16:1200-1207.

40. Pattanayak V, Ramirez CL, Joung JK, Liu DR. Revealing off-target cleavage specificities of zinc-finger nucleases by in vitro selection. *Nat Methods.* 2011;8:765-770.

41. Pennisi E. The CRISPR craze. *Science.* 2013;341:833-836.

ABBREVIATIONS LIST

A1AT	Alpha-1 antitrypsin
AAVS1	adeno-associated virus integration site 1
AFP	Alpha-Fetoprotein
BLI	bioluminescence imaging
CXCR4	chemokine (C-X-C motif) receptor 4
eGFP	enhanced green fluorescent protein
EOMES	Eomesdermin
ESC	embryonic stem cell
Fluc	firefly luciferase
^{68}Ga-DOTATATE	^{68}Ga-DOTA-Tyr^{3}-Thr^{8}-octreotate
HNF4α	Hepatocyte nuclear factor 4 alpha
hNIS	human sodium iodide symporter
hSSTr2	human somatostatin receptor subtype 2
HSV1-TK	herpes simplex virus type 1 thymidine kinase
iPSC	induced pluripotent stem cell
MIXL1	MIX1 homeobox-like protein 1
NANOG	nanog homeobox
OCT4	Octamer-binding transcription factor 4
PET	positron emission tomography
PPP1R12C	protein phosphatase 1, regulatory subunit 12C
SPECT	single photon emission computed tomography
ZFN	zinc finger nucleases

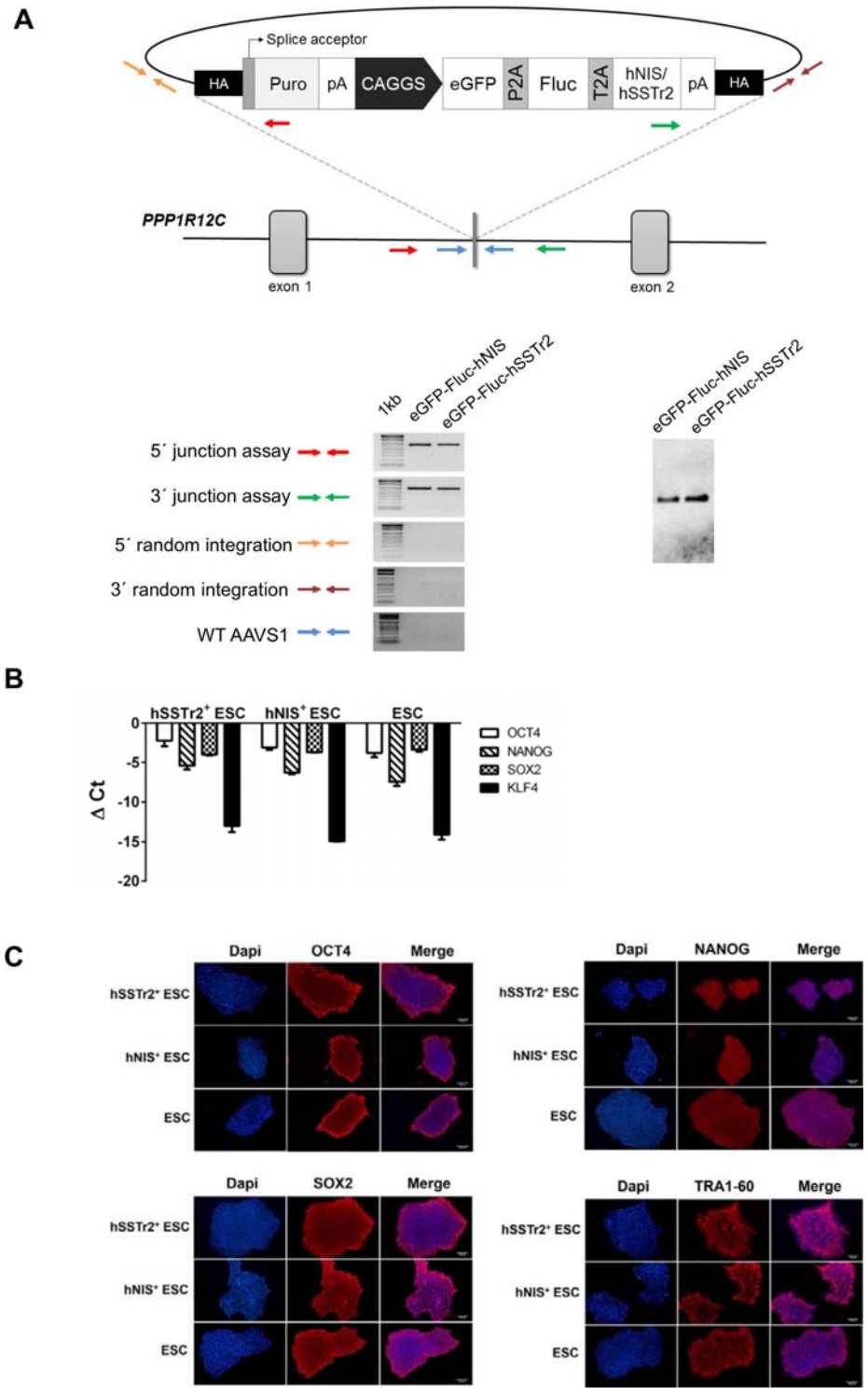

FIGURE 1. Correct integration of the transgenes. Primers used for the 5'/3' junction assay, 5'/3' random integration and WT allele are depicted in red, blue, orange, brown and green. Recombinant lines incorporating transgenes showed correct integration. Southern blot

analysis confirmed correct integration of the construct **(A)**. RT-qPCR showed no significant difference in the expression of pluripotency markers *OCT4, NANOG, SOX2 and KLF4* following genetic engineering (**B**). Immunocytochemistry for *OCT4, NANOG, SOX2 and TRA1-60* showed similar expression in all lines (**C**).

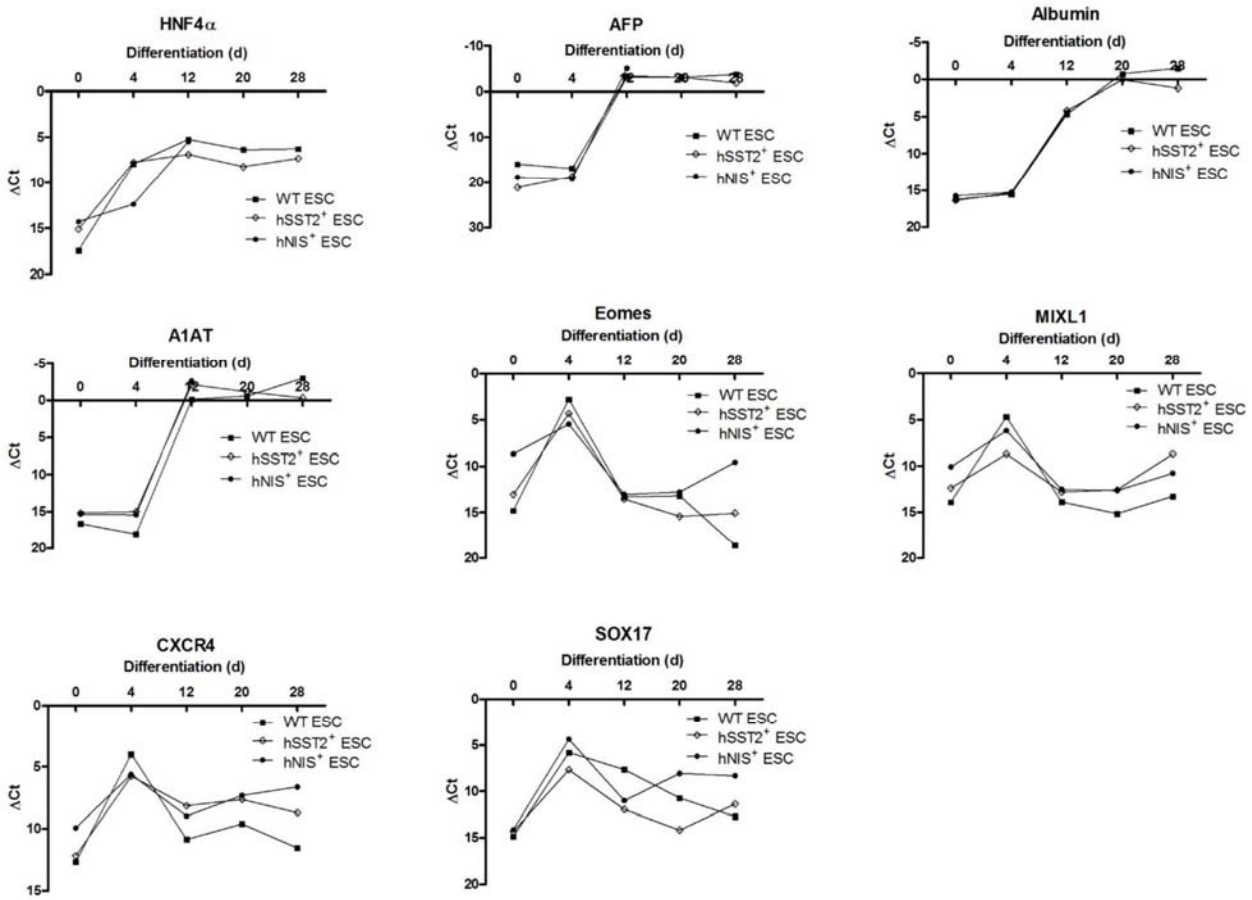

FIGURE 2. No significant difference in hepatic differentiation of hSSTr2^{+}, hNIS^{+} and WT ESC. RT-qPCR for hepatocyte-specific genes HNF4α, AFP, Albumin and A1AT and for definitive endoderm markers EOMES, MIXL1, CXCR4 and SOX17.

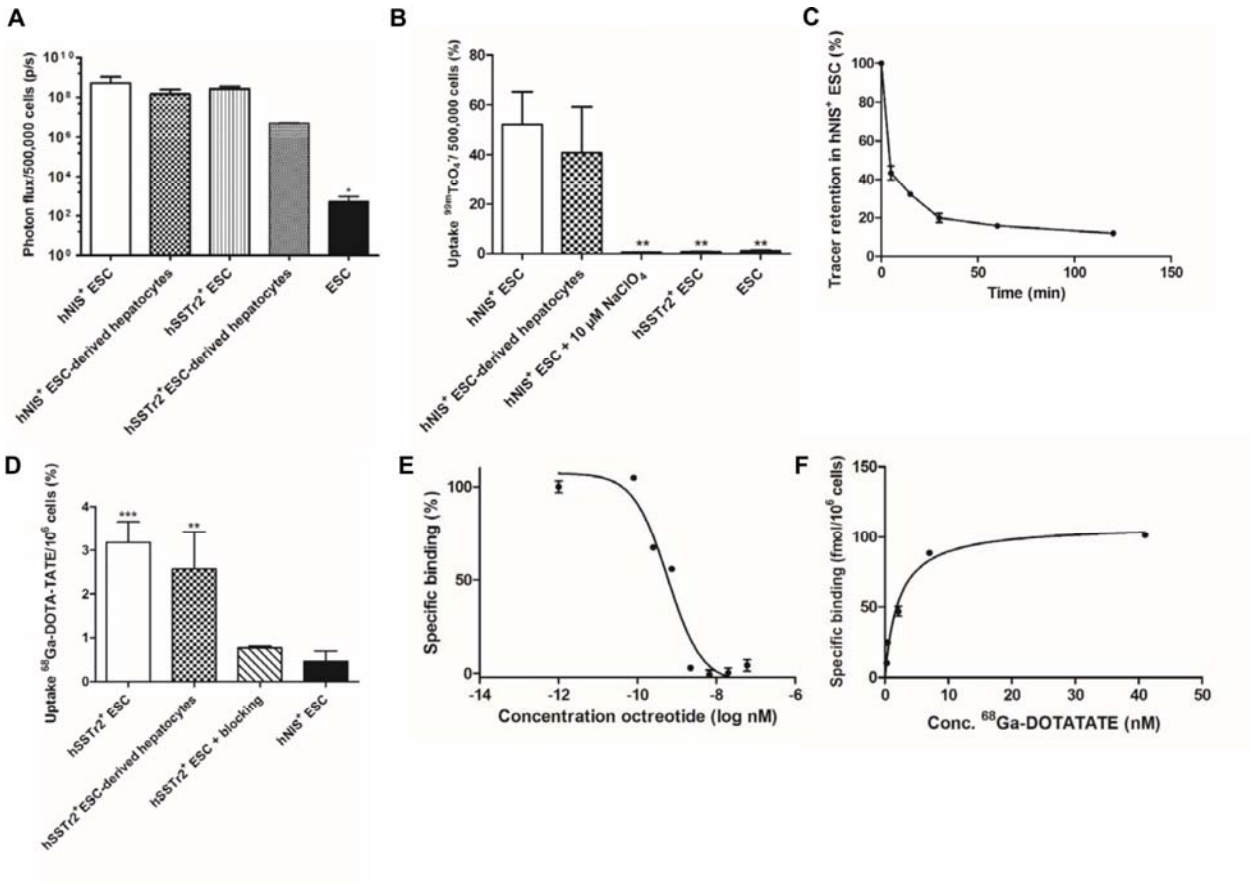

FIGURE 3. *In vitro* BLI signals persisted after hepatic differentiation (**A**). Uptake of $^{99m}TcO_4^-$ by h*NIS*$^+$ ESC persisted after hepatic differentiation and was 50-80 times higher than controls. $NaClO_4$ significantly decreased tracer uptake (**B**). Retention of $^{99m}TcO_4^-$ led to significant tracer elution with ~20% retention (**C**). Binding of ^{68}Ga-DOTATATE in h*SSTr2*$^+$ ESC was significantly higher than controls (h*NIS*$^+$ ESC) and persisted after hepatic differentiation (**D**). Competitive inhibition using octreotide showed an IC_{50} of 0.58nM (**E**). Saturation experiments revealed a Bmax value of 111±5fmol per million cells and Kd of 3.4±0.5nM (**F**). (**p<0.01;***p<0.001)

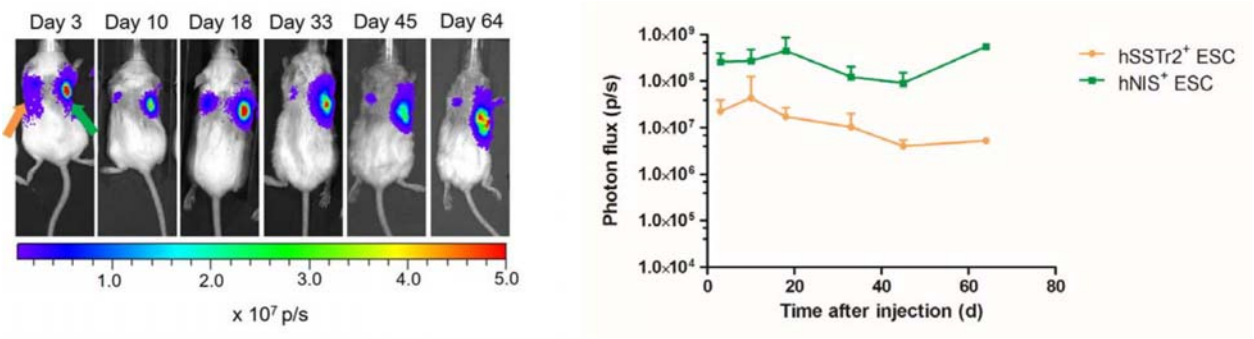

FIGURE 4. BLI of the teratomas showed a clear signal coming from both h*SSTr2*$^{+}$ and h*NIS*$^{+}$ ESC persisting over 70 days.

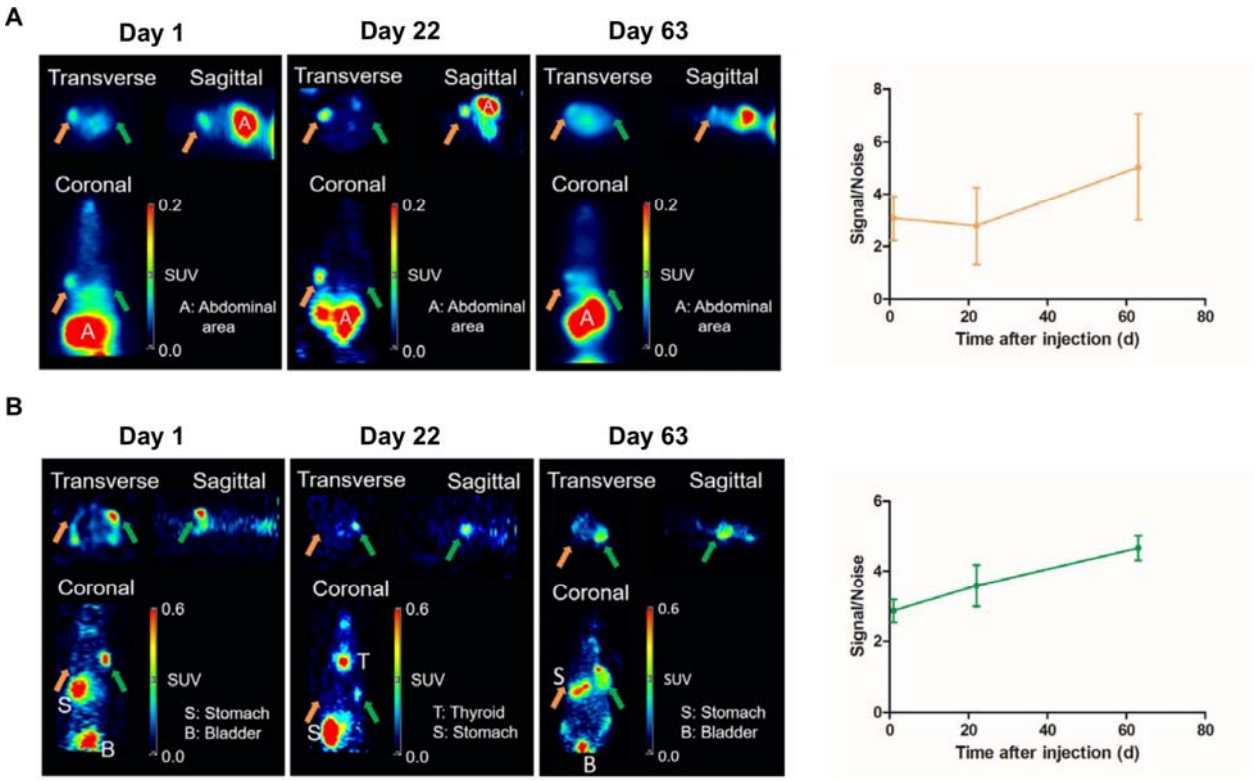

FIGURE 5. PET confirmed tracer uptake at the correct locations. ^{68}Ga-DOTATATE accumulation observed at the h*SSTr2*$^{+}$ ESC site persisted over time (orange arrow), no signal was present at the h*NIS*$^{+}$ ESC graft (green arrow) (**A**). Uptake of $^{124}I^{-}$ at the h*NIS*$^{+}$ ESC site was clear and persisted over time, no signal at the contralateral h*SSTr2*$^{+}$ ESC graft (**B**).

TABLES

TABLE 1. Primers used for PCR genotyping

PCR reaction	Primer sequences
5' junction assay	CACTTTGAGCTCTACTGGCTTC CATGTTAGAAGACTTCCTCTGC
3' junction assay	TTCACTGCATTCTAGTTGTGG AAGGCAGCCTGGTAGACA
5' random integration	GTACTTTGGGGTTGTCCAG TTGTAAAACGACGGCCAG
3' random integration	CCTGAGTTCTAACTTTGGCTC ACACAGGAAACAGCTATGAC
Wild type allele	TTCGGGTCACCTCTCACTCC GGCTCCATCGTAAGCAAACC

TABLE 2. Primers used for RT-qPCR.

Gene	*Forward*	*Reverse*
GAPDH	TCAAGAAGGTGGTGAAGCAGG	ACCAGGAAATGAGCTTGACAAA
EOMES	AACAACACCCAGATGATAGTC	TCATAGTTGTCTCTGAAGCCT
CXCR4	CACCGCATCTGGAGAACCA	GCCCATTTCCTCGGTGTAGTT
MIXL1	GGATCCAGGTATGGTTCCAG	CATGAGTCCAGCTTTGAACC
SOX17	CGCTTTCATGGTGTGGGCTAAGGACG	TAGTTGGGGTGGTCCTGCATGTGCTG
HNF4a	ACTACGGTGCCTCGAGCTGT	GGCACTGGTTCCTCTTGTCT
AFP	TGAGCACTGTTGCAGAGGAG	GTGGTCAGTTTGCAGCATTC
ALB	ATGCTGAGGCAAAGGATGTC	AGCAGCAGCACGACAGAGTA
A1AT	AGGGCCTGAAGCTAGTGGAT	TCCTCGGTGTCCTTGACTTC

Online supplemental files

MATERIALS AND METHODS

^{68}Ga-DOTATATE preparation

^{68}Ga-DOTATATE was prepared by heating gallium-68 chloride (400-800MBq) at pH4-4.4 with 30µg DOTATATE (Bachem, Switzerland) (adapted from (*1*)). ^{68}Ga-chloride was obtained by elution of a germanium-68/gallium-68 generator with diluted HCl-solution followed by purification over a Dowex column (Sigma-Aldrich/Fluka, St. Louis, Missouri). The reaction mixture was purified over a Sep-Pak C18 column and formulated into a clinical-grade injectable solution.

FIGURES

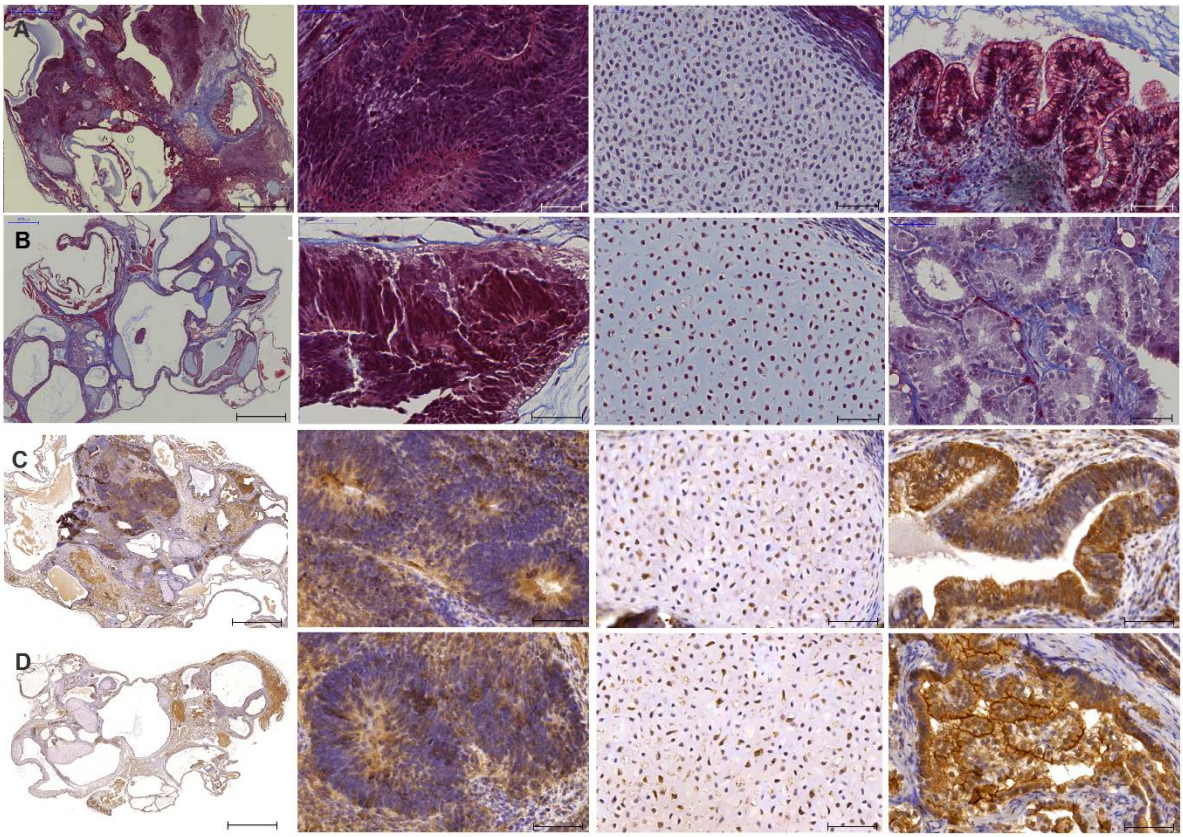

Online supplemental Figure 1. Histological validation of teratoma formation. Teratomas derived from hSSTr2+ ESC (**A**). Differentiation towards neural rosettes, cartilage and intestinal lining epithelium. hNIS+ teratoma (**B**) differentiation towards neural rosettes, cartilage and glandular tissue. Immunohistochemistry for hSSTr2 was positive in hSSTr2+ teratomas (**C**). Immunohistochemistry for hNIS was positive in the hNIS+ teratoma (**D**). Scale bar overviews:1000µM. Others:50µM.

ONLINE SUPPLEMENTAL REFERENCES

1. Van Binnebeek S, Vanbilloen B, Baete K, et al. Comparison of diagnostic accuracy of (111)In-pentetreotide SPECT and (68)Ga-DOTATOC PET/CT: A lesion-by-lesion analysis in patients with metastatic neuroendocrine tumours. *Eur Radiol.* 2016;26:900-909.